Turbulent Dispersion from Elevated Line Sources in Channel and Couette Flow

Phuong M. Le
School of Chemical Engineering and Materials Science, The University of Oklahoma, Norman, OK 73019

Dimitrios V. Papavassiliou
Sarkeys Energy Center, The University of Oklahoma, Norman, OK 73019

DOI 10.1002/aic.10507
Published online June 17, 2005 in Wiley InterScience (www.interscience.wiley.com).

Turbulent dispersion of a scalar emitted from a source in homogeneous turbulence has been placed in a solid theoretical context by Taylor, Saffman, and Batchelor. However, the case of source diffusion in the near-wall region, where the turbulence is not Gaussian, and the effects of the molecular Prandtl number (Pr) on the effective dispersion have not been explored to similar depth. The present work studies the behavior of elevated sources in turbulent channel flow and in turbulent-plane Couette flow. The trajectories of heat markers are monitored in space and time as they move in a hydrodynamic field created by a direct numerical simulation. The fluids span several orders of magnitude of Pr (or Schmidt number), Pr = 0.1, 0.7, 3, 6, 10, 100, 200, 500, 1000, 2400, 7500, 15,000, and 50,000 (liquid metals, gases, liquids, lubricants, and electrochemical fluids). It is found that the molecular Pr has negligible effects in the evolution of the marker cloud for Pr ≥ 3, when the point of marker release is away from the viscous wall sublayer. However, when the markers are released close to the wall, the molecular effects on dispersion are strong. It is also found that total effective dispersion is higher in the case of plane Couette flow, where the total stress across the channel is constant. © 2005 American Institute of Chemical Engineers *AIChE J,* 51: 2402–2414, 2005
Keywords: turbulent transport, Lagrangian methods, source diffusion

Introduction

The prediction of turbulent dispersion of a scalar contaminant emitted from sources above a surface is a problem that gained importance recently because of its application in atmospheric pollution and in the dispersion of bioagents in the case of an act of terrorism. The statistical description of turbulent dispersion from a Lagrangian perspective was introduced by Taylor,[1] who described the rate of dispersion of fluid particles from a point source in homogeneous, isotropic turbulence as

$$\frac{d\overline{X_f^2}}{dt} = 2\overline{u^2}\int_0^t R^L(\tau)d\tau \tag{1}$$

where X_f is the displacement of a fluid particle relative to its source, $\overline{u^2}$ is the mean square of the x-component of the velocity of the fluid particles, and R^L is the Lagrangian correlation coefficient. Taylor's equation can be seen as an extension of Einstein's relation[2] for the dispersion of particles with Brownian motion, given as

$$d\overline{X_p^2}/dt = 2D \tag{2}$$

where X_p is the displacement of a particle relative to its source and D is the molecular diffusivity. Saffman[3] studied the effects

D. V. Papavassiliou is also affiliated with the School of Chemical Engineering and Materials Science, The University of Oklahoma, Norman, OK 73019.
Correspondence concerning this article should be addressed to dvpapava@ou.edu.

of molecular diffusion on turbulent dispersion and developed a relation for dispersion in this case by defining a material autocorrelation function, which correlated fluid velocity components along the trajectories of scalar markers instead of fluid particles. Saffman argued that scalar markers can move off a fluid particle as a result of molecular diffusion, and thus the effect of molecular diffusion is to diminish turbulent diffusion because the markers do not follow the chaotic turbulent fluid motion. With respect to anisotropic turbulent flows, Batchelor[4] developed a theory for the prediction of the statistical behavior of a source in a turbulent boundary layer. Batchelor[4] argued (based on similarity) that the Lagrangian velocity within the constant stress region depends only on the friction velocity u^* and time so that

$$\overline{V_y} \equiv \frac{d\bar{Y}}{dt} = bu^* \tag{3}$$

where b has to be an absolute constant, independent of molecular diffusion effects.

Laboratory measurements for turbulent dispersion have been reported for the case of continuous elevated sources of a passive scalar.[5,6] Shlien and Corrsin[5] examined turbulent dispersion of heat in a wind tunnel, downstream from a heated wire, and Fackrell and Robins[6] studied turbulent mass dispersion with emphasis on the concentration fluctuations using propane as a tracer gas. More recently, direct numerical simulations (DNS) of turbulent flows in conjunction with tracking of scalar markers have been used for the investigation of scalar dispersion in anisotropic turbulent flows.[7-10] However, emphasis has been given to sources located at the solid surface. Papavassiliou[11] studied the effects of the molecular Prandtl number (Pr) on the evolution of a cloud of markers released instantaneously from a line source at the wall of a channel (that is, a puff) for $0.1 \leq \mathrm{Pr} \leq 50{,}000$. The puff was found to develop in the following three stages:

- Zone I, in which molecular diffusion dominates dispersion.
- Zone II, which is a transition zone.
- Zone III, in which turbulent convection dominates dispersion.

The extent of Zones I and II depends on the Pr; it becomes longer as the Pr increases. Mitrovic and Papavassiliou[9] calculated the turbulent transport properties for the plume that results from a continuous line source at the wall, and modeled its behavior for $0.1 \leq \mathrm{Pr} \leq 50{,}000$. They found that the behavior of the plume exhibits three zones of development, which correspond directly to the three stages of development of a puff. The behavior of both puffs and plumes that are emitted from wall sources was found to be Pr dependent.

The present study explores the effects of molecular diffusion on turbulent transport for the case of elevated sources from the wall, and the effects of turbulence structure on turbulent dispersion. The effects of molecular diffusion are explored by changing the Pr of the fluid, and the effects of the turbulence structure are investigated by placing the sources in a plane channel flow and in a plane Couette flow. In plane Couette flow, the driving force for the flow is the shear effect of the two channel walls moving in directions opposite to each other. The total stress is constant across the whole channel, creating a very extensive constant stress region, similar to the logarithmic region in Poiseuille channel flow. Thus, we can achieve a wide logarithmic layer that is computationally difficult to obtain otherwise (that is, with a DNS of plane channel flow). A tracking algorithm is used to monitor the trajectories of scalar markers in space and time as they move in the hydrodynamic field created by a DNS. The fluids span several orders of magnitude of Pr [or Schmidt number (Sc)], Pr = 0.1, 0.7, 3, 6, 10, 100, 200, 500, 1000, 2400, 7000, 15,000, 50,000 (liquid metals, gases, liquids, lubricants, and electrochemical fluids).

Lagrangian Scalar Tracking

The basic concept of Lagrangian scalar tracking (LST) is that passive scalar transport in turbulent flow is the result of the combined behavior of an infinite number of continuous sources of heat or mass markers, such as the markers discussed by Saffman.[3] Hanratty[12] used this concept to describe the transfer of heat from a hot to a cold wall in turbulent channel flow. The study of heat or mass transfer using such an approach has become feasible with the development of appropriate numerical methodologies and the appearance of supercomputers.[13] Papavassiliou and Hanratty[8,14] used a DNS in conjunction with the tracking of scalar markers to study heat transfer based on direct calculations of the behavior of such wall sources. More about the implementation and validation of the LST methodology, which includes the stochastic tracking of heat or mass markers in a turbulent flow field, and the statistical postprocessing of the results to obtain scalar profiles, can be found elsewhere.[8,10,15,16] Heat transfer across the interface between a turbulent gas and a turbulent liquid has also been simulated using LST.[17,18]

For the present study, the trajectories of heat or mass markers in the flow field created by a DNS were calculated using the tracking algorithm of Kontomaris et al.[13] The marker motion was partitioned into a convective part and a molecular diffusion part. The convective part was calculated from the fluid velocity at the particle position yielding for the equation of particle motion $\vec{V}(\vec{x}_o, t) = [\partial \vec{X}(\vec{x}_o, t)]/\partial t$, where the Lagrangian velocity of a marker released at location $\vec{x}_o$ is given as $\vec{V}(\vec{x}_o, t) = \vec{U}[\vec{X}(\vec{x}_o, t), t]$ ($\vec{U}$ is the Eulerian velocity of the fluid at the location of the marker at time t). The effect of molecular diffusion follows from Einstein's theory for Brownian motion (see Eq. 2); the diffusion effect was simulated by adding a three-dimensional random walk on the particle motion at the end of every convection step. The size of the random jump in each one of the three space directions took values from a Gaussian distribution with zero mean and a standard deviation of $\sigma = \sqrt{2\Delta t/\mathrm{Pr}}$ in wall units. Effects of Pr on the process can thus be studied by modifying σ. This allows the LST methodology to simulate fluids within an extensive range of Pr. In contrast, Eulerian simulations for heat transfer in the case of anisotropic turbulence (that is, channel or Couette flow) have been limited to a narrower range of fluids with molecular Pr or Sc between 0.025 and 10,[†] because, to resolve all the scales of motion and temperature, the number of grid points has to be analogous to $\mathrm{Pr}^{3/2}$.[19-26] In the case of homogeneous and isotro-

[†] To our knowledge, there is no published Eulerian DNS work for anisotropic flow and Pr > 10, even though Tiselj's group (2002) at the Institute Jozef Stefan has accomplished DNS with at least Pr = 54.

pic turbulence, however, recent Eulerian DNS have examined cases of relatively high Sc.[27] Yeung et al.[28] examined the case of $0.125 \leq Sc \leq 64$, and Nieuwstadt and Brethouwer[29] and Brethouwer et al.[30] studied the range of $0.04 \leq Sc \leq 144$. Finally, the markers used here are assumed to be passive and thus have no effect on the flow.

Direct Numerical Simulations

The behavior of a scalar source was determined by following the paths of a large number of scalar markers in a flow field created by a DNS (see Lyons et al.[31] and Günther et al.[32] for the validation of the channel flow DNS used in this study; and Papavassiliou and Hanratty[33] for the methodology implemented for the Couette flow DNS used in this study). The flow was for an incompressible Newtonian fluid with constant physical properties. In the case of channel flow, it was driven by a constant mean pressure gradient, and for the case of plane Couette flow it was driven by the shear motion of the two moving walls of the channel. The Reynolds number, defined with the centerline mean velocity and the half-height of the channel for the Poiseuille flow channel, and defined with half the velocity difference between the two walls and the half channel height for the Couette flow channel, was 2660 for both. For the Poiseuille channel, the simulation was conducted on a $128 \times 65 \times 128$ grid in x, y, z, and the dimensions of the computational box were $4\pi h \times 2h \times 2\pi h$, where $h = 150$ in wall units.[‡] For the Couette flow channel, the simulation was conducted on a $256 \times 65 \times 128$ grid, and the dimensions of the computational box were $8\pi h \times 2h \times 2\pi h$, where $h = 153$. The flow was regarded as periodic in the x and z directions, with the periodicity lengths equal to the dimensions of the computational box in these directions. The Couette flow channel was chosen to be longer than the Poiseuille channel to minimize the effects of the large-scale structures known to be present in Couette flow simulations.[33,34] First- and second-order turbulence statistics for the flow fields are presented in Figure 1. The mean velocity profile is shown in Figure 1a, and the turbulence intensities are shown in Figure 1b for the x, y, and z directions. Experimental and numerical data obtained in other previous studies for the case of Couette flow are included in these figures to demonstrate the behavior of that simulation. The time step for the calculations of the hydrodynamic field and the Lagrangian tracking was $\Delta t = 0.25$ and $\Delta t = 0.2$ for the Poiseuille and Couette channels, respectively. Both simulations were first allowed to reach a stationary state before the heat markers were released.

Results and Discussion

Table 1 presents a summary of the runs conducted for the current study. Runs P1 to P14 tracked markers in a Poiseuille flow channel with Pr = 0.1, 0.7, 3, 6, 10, 100, 200, 500, 1000, 2400, 7500, 15,000, and 50,000 up to time $t = 300$. In each one of these runs, a total of 16,129 markers were released instantaneously from a uniform rectangular grid that covered the x–z plane of the computational box at different distances from the wall. The choices of these distances were the edge of the

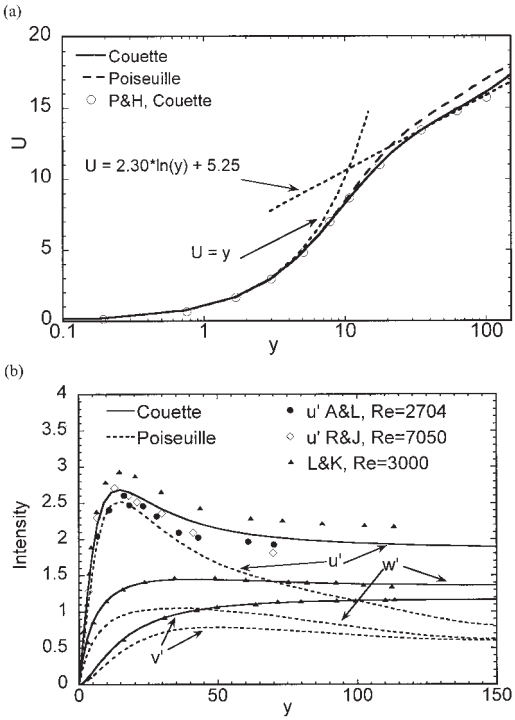

Figure 1. Turbulent flow statistics.

(a) Mean velocity profile, (b) turbulence intensity in the streamwise, normal, and spanwise flow directions. [P&H = Papavassiliou and Hanratty[33]; L&K = Lee and Kim[44]; A&L = Aydin and Leutheusser[45]; R&J = Robertson and Johnson.[46]]

thermal sublayer (that is, $y_o = 5$ for $Pr \leq 1000$, $y_o = 1$ for $Pr > 1000$), the region of transition between the viscous sublayer and the logarithmic velocity layer (that is, $y_o = 15$), a point at $y_o/h \approx 0.2$ to compare with the experimental measurements of Fackrell and Robins[6] for elevated sources at Pr = 0.7, a point in the logarithmic region (that is, $y_o = 75$), and a point at the center of the channel. Runs C1 to C12 tracked markers for similar conditions in a plane Couette flow, where the main difference was that 145,161 markers were tracked.

The initial marker positions were on a uniform 127×127 grid and a 381×381 grid for the Poiseuille flow and Couette flow, respectively. For plane channel flow, Mitrovic and Papavassiliou[9,35] found that using more markers than the 127×127 case (one order of magnitude more) in the flow improves the calculation of statistics only slightly, so the use of 16,129 markers is sufficient for the plane channel case. The computational box is twice as large for the plane Couette flow, and one order of magnitude more markers are used in that case.

Instantaneous line source behavior

The cloud that results from an instantaneous source of a scalar is usually called a *puff* and the cloud that results from a continuous source of a scalar is called a *plume*. Figure 2a presents the mean puff trajectory in the normal direction for the marker cloud of runs P2 and P3, and Figure 2b for the marker cloud of run C2 (Pr = 0.7 in these cases, corresponding to dispersion of heat in air). Physically, this is the trajectory of the centroid of a puff of markers released from an instantaneous

[‡] All quantities in this work are expressed in viscous wall units unless otherwise specified.

Table 1. Summary of the Conditions Applied to the Simulation Runs Used in This Work*

Run Number	Pr	Source Elevation from the Wall in Viscous Wall Units					Numbers of Markers
		Case a	Case b	Case c	Case d	Case e	
P1	0.1	5	15	28.5	75	150	16,129
P2	0.7	5	15	28.5	75	150	16,129
P3	0.7	2	38.5	50	96	125	16,129
P4	3	5	15	28.5	75	150	16,129
P5	6	5	15	28.5	75	150	16,129
P6	10	5	15	28.5	75	150	16,129
P7	100	5	15	28.5	75	150	16,129
P8	200	5	15	28.5	75	150	16,129
P9	500	2	15	28.5	75	150	16,129
P10	1000	5	15	28.5	75	150	16,129
P11	2400	1	15	28.5	75	150	16,129
P12	7500	1	15	28.5	75	150	16,129
P13	15,000	1	15	28.5	75	150	16,129
P14	50,000	1	15	28.5	75	150	16,129
C1	0.1	1	15	28.5	75	150	145,161
C2	0.7	1	15	28.5	75	150	145,161
C3	6	1	15	28.5	75	150	145,161
C4	10	1	15	28.5	75	150	145,161
C5	100	1	15	28.5	75	150	145,161
C6	200	1	15	28.5	75	150	145,161
C7	500	1	15	28.5	75	150	145,161
C8	1000	1	15	28.5	75	150	145,161
C9	2400	1	15	28.5	75	150	145,161
C10	7500	1	15	28.5	75	150	145,161
C11	15,000	1	15	28.5	75	150	145,161
C12	50,000	1	15	28.5	75	150	145,161

Each run was for a different Pr and a different flow field (the letter P in the run number indicates Poiseuille flow and the letter C indicates Couette flow). Passive markers were released at five different elevations in each of the flow fields, indicated by the letters a–e. Each simulation was run for 300 viscous time units.

line source located at different distances y_o from the channel wall. It is observed that the marker clouds tend to move away from the wall in both cases. The reason for this effective diffusion of markers away from the wall, even though the probability of moving toward the wall or away from it is the same for each marker, is that there are initially many more markers close to the wall. Thus, the number of markers that can go away from the wall is larger than those going toward the wall from the outer region because there are not that many markers in the outer region of the flow. As a result, the net number of markers moving away from the wall is positive, and the cloud centroid moves away from the wall. It is also observed that the centroid of the puff in the Couette flow environment is moving away from the wall much faster than in the Poiseuille flow environment. Figure 1b shows that the root mean square of the vertical velocity fluctuations is higher in Couette flow than that in channel flow, meaning that stronger fluctuations can take markers away from the wall. Na et al.[36] studied large-scale structures that produce Reynolds stresses and look like sheets extending well into the logarithmic region (which they called "super-bursts"). Because Couette flow is a very large constant stress region, such structures are also present in Couette flow, resulting in higher rates of dispersion away from the wall. This appears to be a difference in the fundamental mechanism of heat convection in the log layer and in channel flow.

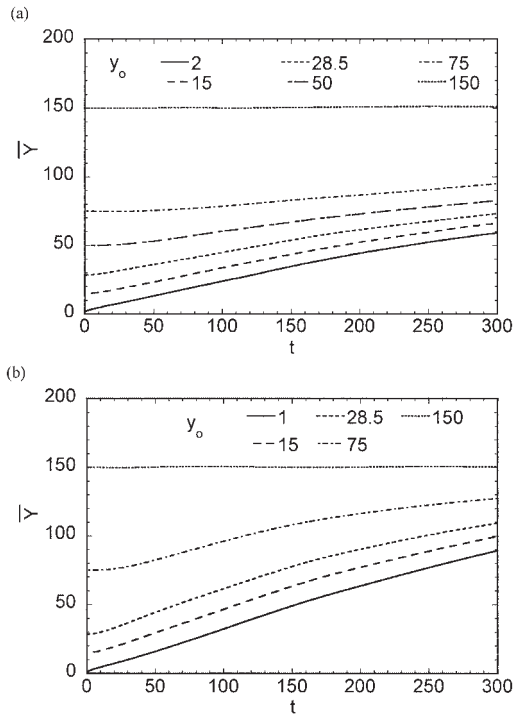

Figure 2. Mean puff normal position for different source elevations as a function of time for Pr = 0.7.

(a) Poiseuille flow; (b) Couette flow.

The density of the cloud of the markers is represented by the probability, $P_1(\vec{x}, t \mid \vec{x}_o, t_o)$, of a marker to be at a location $\vec{x} = (x, y, z)$ in the flow field at time t, given that it was released at location $\vec{x}_o = (x_o, y_o, z_o)$ at time t_o. This probability can be interpreted physically as concentration[3] and thus as a snapshot of a cloud of contaminants released instantaneously from $\vec{x}_o$. Figures 3 and 4 present contours of the puff concentration for Poiseuille and Couette flows, respectively, and for Pr equal to 0.7 and to 200 (runs P2, P8, C2, and C6). The point of release

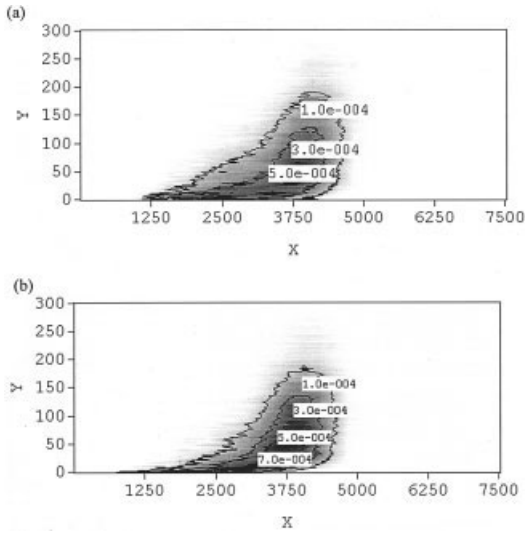

Figure 3. Contour plot for the concentration profile resulting from a puff in channel flow for at $t^+ = 300$ and source elevation of $y_o = 28.5$.

(a) Pr = 0.7; (b) Pr = 200.

is $y_o = 28.5$ in both cases. In both types of flow the effect of increasing the Pr is similar; the cloud of markers is more concentrated around the point of release. For small Pr the markers disperse faster to other areas of the flow field arising from bigger molecular jumps, whereas for higher Pr, a larger percentage of markers stay close to the point of release for longer times. However, for sources at higher elevations (not shown here) there are no major differences in the puff concentration for different Pr number fluids. The behavior of the Poiseuille flow markers and the Couette flow markers is similar

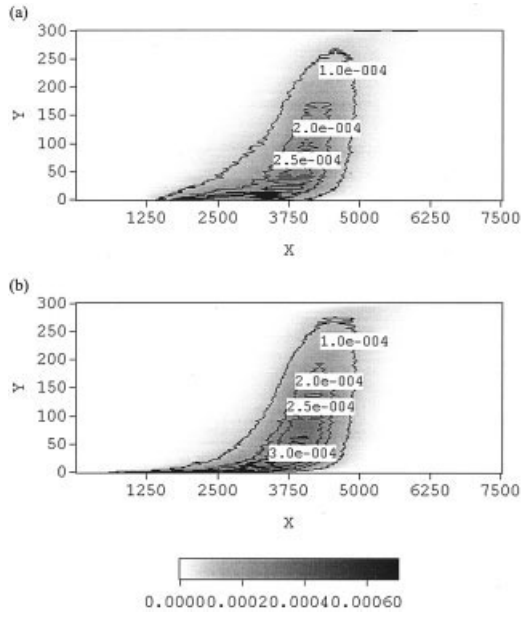

Figure 4. Contour plot for the concentration profile resulting from a puff in Couette flow for at $t^+ = 300$ and source elevation of $y_o = 28.5$.

(a) Pr = 0.7; (b) Pr = 200.

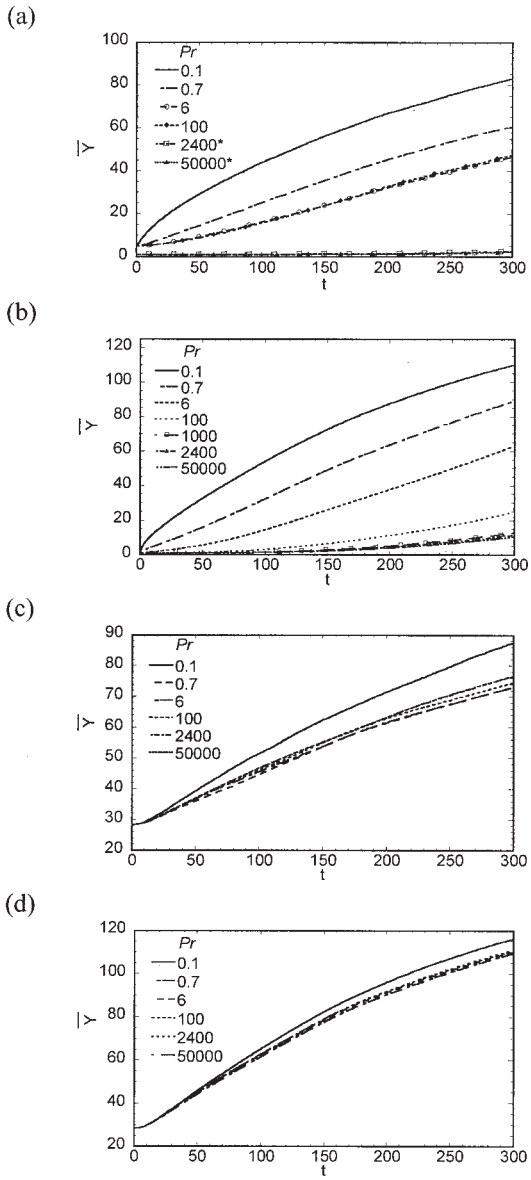

Figure 5. Mean puff normal position for different Pr as a function of time.

(a) Poiseuille flow (* $y_o = 1$, no asterisk $y_o = 5$); (b) Couette flow, $y_o = 1$, (c) Poiseuille flow, $y_o = 28.5$; (d) Couette flow, $y_o = 28.5$.

in this respect. Figure 4 shows that the dispersion of the puff in the normal direction is higher for Couette flow than for plane channel flow. The reason is the same as for the case of the faster $\bar{Y}$ movement away from the wall observed in Figure 2, that is, larger-velocity fluctuations in the vertical direction for Couette flow and larger-scale flow structures extending in the outer region result into higher dispersion.

The mean cloud trajectories in the normal direction are shown in Figure 5 for different Pr. Figures 5a and 5b present the trajectories of clouds released at the edge of the thermal conductive sublayer for channel and Couette flows, respectively. The effects of the fluid Pr are evident in these figures: the plane channel puffs become Pr independent for Pr $\geq$ 6 and the plane Couette flow puffs for Pr $\geq$ 1000. Figures 5c and 5d

show the trajectories of clouds released within the transition region. For both channel flow and Couette flow, the effects of Pr are negligible for release locations in the outer region of the flow. Only in the case of Pr = 0.1 in channel flow does it behave in a manner different from that of the other cases. The same behavior is found for puffs released at locations farther from the wall (not shown here). The reason for this behavior can be explored, if one considers the relative magnitude of the eddy diffusivity and the molecular diffusivity. Fluids with molecular Pr on the order of magnitude of ≤ 1 have molecular diffusivities that are comparable to or higher than the eddy diffusivity, and thus Pr effects are expected to be observed. To illustrate this point, we can review published values of the turbulent Pr and estimate the order of magnitude of the eddy diffusivity using them. Results from direct numerical simulations for turbulent heat transfer in a channel,[20-22,37,38] from large eddy simulations,[39] and from modeling correlations[40,41] suggest that the value of the turbulent Pr is on the order of one for different molecular Pr. The turbulent Pr for wall turbulence is a function of the distance from the wall (as are the eddy viscosity and the eddy diffusivity), but in terms of order of magnitude it varies only slightly for $y > 10$. The eddy viscosity for the flow field under consideration here is on the order of 10,[8] in the outer region of the flow ($y > 30$), which means that the eddy diffusivity is on the order of 10 as well. Both DNS[20] and experiments[42] agree with this estimation (in terms of order of magnitude). Because the fluid viscosity is one, a fluid with molecular Pr = 1 has diffusivity of one and a fluid with molecular Pr = 0.1 has diffusivity of 10, which is comparable to the eddy diffusivity.

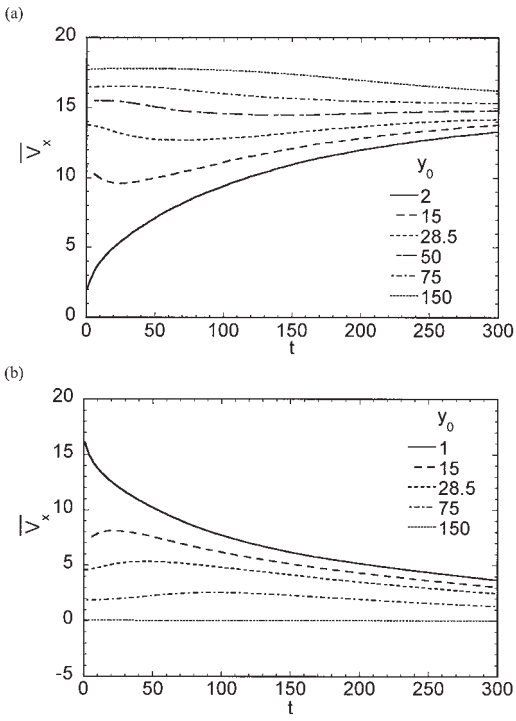

Figure 6. Mean puff streamwise velocity for different source elevations as a function of time for Pr = 0.7.

(a) Poiseuille flow; (b) Couette flow.

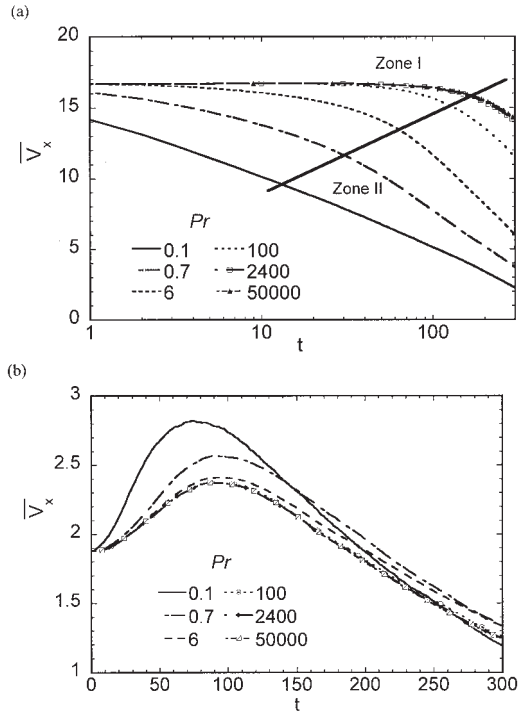

Figure 7. Mean puff streamwise velocity for different Pr as a function of time for Couette flow.

(a) $y_o = 1$; (b) $y_o = 75$.

The mean streamwise velocity of the puff $\bar{V}_x$ is shown in Figure 6 for different elevations and Pr = 0.7. This velocity is expected to reach the value of the bulk mean velocity of the flow field (which is 15.1 in wall units for channel flow and 0 for Couette flow) at long times because the markers are expected to disperse uniformly across the channel at long times. Figure 6a shows that the mean puff velocity drops for elevations higher than $y_o = 10$ because the markers start to disperse to regions where the mean velocity is smaller than the mean velocity at the point of release. Similarly, for Couette flow, the mean puff velocity shows a maximum for elevations between the viscous sublayer and the center of the channel because the markers disperse to areas of higher mean velocity before uniformly covering the channel.

Figures 7a and 7b present the mean streamwise velocity as a function of Pr for the case of Couette flow and for source location in the viscous sublayer and in the outer region, respectively. The conclusions reached above based on the puff trajectories also apply here; the effects of Pr are important for sources within the viscous sublayer, as seen in Figure 7a, whereas they are not for sources farther away unless the Pr is small (Pr < 10). Figure 7a shows the first two zones of plume development for high Pr, similar to those observed by Mitrovic and Papavassiliou,[9] for sources on the channel wall. In the first zone, the markers move as a result of molecular dispersion and in the second zone the contributions of convection begin to appear. The transition point between these zones is Pr dependent.

Figures 8a and 8b present the mean normal velocity as a function of Pr for the Couette flow case and for source locations in the viscous sublayer ($y_o = 1$) and in the outer region (y_o

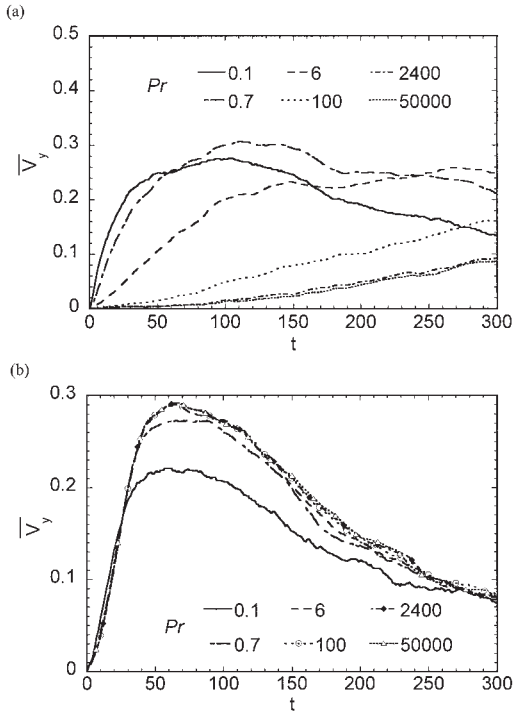

Figure 8. Mean puff normal velocity for different Pr as a function of time for Couette flow.

(a) $y_o = 1$, (b) $y_o = 75$.

$= 75$). Figure 8 shows that the velocity $\bar{V}_y$ is a function of time and of Pr. It is observed that $\bar{V}_y$ reaches a maximum when the movement of the markers is restricted by the channel wall, and beyond that point tends to the value of 0. It is also observed that the assumption that the Lagrangian velocity of scalar markers is constant within the constant stress region and independent of Pr is not accurate, and therefore a universal constant b (see Eq. 3) cannot describe all dispersion cases.

Continuous line source behavior and comparison to experiments

The behavior of a plume originating at $\vec{x_o}$ and emitting markers from time t_o to time t_f can be simulated by integrating the probability density function that describes the behavior of the puffs

$$P_2(X - x_o,\, Y,\, t_f) = \sum_{t=t_o}^{t_f} P_1(X - x_o,\, Y,\, t|\vec{x_o},\, t_o) \qquad (4)$$

The probability P_1 was calculated for each Pr using a grid that covers the flow domain and counting the number of markers that are present in each grid cell.[16] The grid in the normal direction was constructed by uniformly dividing the width of the channel into 300 bins. In the streamwise direction, the grid was stretched to take measurements at long distances downstream from the source. The stretching in the streamwise direction followed the relation $\Delta x_n = 1.06^n \Delta x_o$ with $\Delta x_o = 5$.

The DNS/LST methodology has been validated with experimental data for the case of continuous wall sources.[9,11] Here, we present comparisons with experiments for the case of elevated scalar sources. Fackrell and Robins[6] measured mean concentration profiles for a passive plume from an elevated source within a turbulent boundary layer. The source location was at $y_o/h \approx 0.2$ (note that h is the boundary layer thickness at the source location for the Fackrell–Robins experiments) and the source gas consisted of a mixture of propane and helium, the former being used as a trace gas for concentration measurements. They calculated the plume half-width (δ_y), which is defined to be the distance from the location of maximum concentration at which the concentration falls to half of its maximum. Figure 9 presents a comparison of the experimental measurements with the DNS/LST results showing very good agreement between the two cases. Figure 10a presents the mean concentration profile normalized with the maximum concentration at different distances downstream from the source. The agreement between the experiments and the DNS/LST results is also quite good. Figure 10b shows a comparison with the experiments of Shlien and Corrsin,[5] in which dispersion within a turbulent boundary layer was measured downstream of a heated wire located at different elevations from the wall. Heat was supplied to the wire at a constant rate, so that their case is equivalent to the calculation of P_2 profiles using LST. They scaled the distance from the wall and the distance downstream from the source with the displacement thickness of the momentum turbulent boundary layer (δ_d) at the location of the tagging wire. To calculate the appropriate length scale for the channel flow DNS, the mean centerline velocity of the channel is used in place of the free stream velocity for the calculation of the boundary layer thickness. The calculated value for the DNS is $\delta_d = 23.2$. Figures 9 and 10 indicate that the DNS/LST data are reliable for the calculation of the properties of elevated scalar sources.

Figures 11a–11c show the plume half-width for plane channel flow and different source elevations for all Pr considered. It appears that the Pr affects the development of the plume for sources within the viscous wall region, but the plume becomes Pr independent for sources farther from the wall. The reason for this is that turbulent dispersion is dominant in the outer region relative to the molecular diffusion. The development of δ_y follows a relation of the form

$$\delta_y/h = a(x/h)^c \qquad (5)$$

According to the statistical theory of turbulent dispersion[43] the dispersion of the plume in the normal direction is predicted to

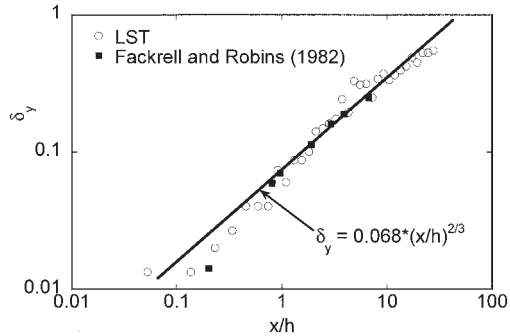

Figure 9. Comparison of the plume half width computed with the DNS/LST method and experiments.

The value of R^2 for the line shown is 0.945.

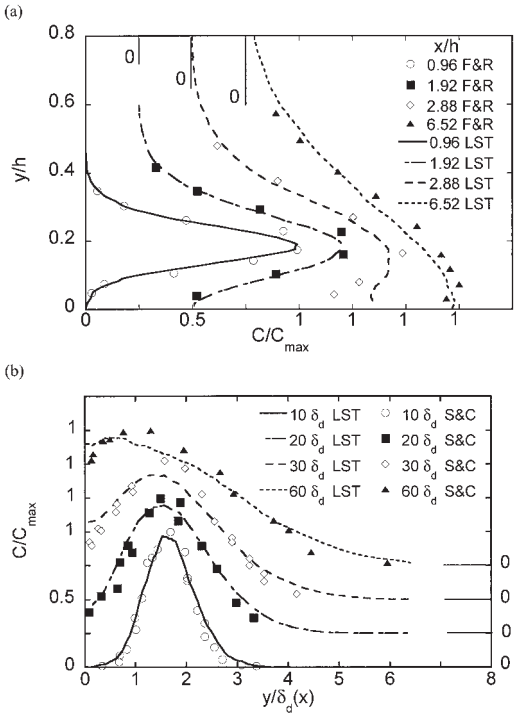

Figure 10. Comparison of the concentration profile resulting from an elevated source with the DNS/LST method and experimental measurements.

(a) Comparison to the mass transfer experiments of Fackrell and Robins[6]; (b) comparison to heat transfer experiments by Shlien and Corrsin.[5]

be $\overline{Y^2} = [\overline{v^2}/(\bar{U})^2]x^2$ for small times and $\overline{Y^2} = 2\tau_L[\overline{v^2}/(\bar{U})^2]x$ for long times, where τ_L is the Lagrangian timescale and $\overline{v^2}$ is the mean square of the velocity fluctuations in the normal direction. Thus, one would expect the exponent in Eq. 5 to be $c = 1/2$ (because in the present case the plume is allowed to develop for long times). However, the turbulence in channel flow is not homogeneous, and $\overline{v^2}/(\bar{U})^2$ can be assumed to change with the distance from the wall according to a function $(y/h)^b$ with $b > 0$ up to $y \approx 50$, implying that $c = 1/(2 - b) \geq 1/2$.

The results show that for sources within the conductive sublayer, the development of δ_y is initially proportional to $(x/h)^{1/2}$ and proportional to $(x/h)^{3/2}$ at larger distances from the source. It is also noted that the $(x/h)^{1/2}$ region is longer for smaller Pr (Figure 11a). For sources within the transition region and for Pr > 10, the behavior of δ_y is better described with two equations (Figure 11b): one for the region near the source ($x/h < 10$) and one for the region far from the source ($x/h > 10$). For sources outside the viscous wall region, the behavior of δ_y can be described with one equation for Pr ≥ 3 (see Figure 11c). Figures 12a–12c present the plume half-width for the Couette flow channel. Similar to Poiseuille flow, Eq. 5 is found to describe the data. For sources within the conductive sublayer, $\delta_y \sim (x/h)^{2/3}$ initially, and $\delta_y \sim (x/h)^{3/2}$ at larger distances from the source (Figure 12a). The half-plume growth rate, for Couette flow sources outside the viscous layer, exhibits an exponential dependency on x/h similar to that for the plane channel case. However, as seen from Figures 12b and 12c, the values of the parameter a are higher for Couette flow, indicating a higher dispersion rate for the Couette flow plumes.

Correlation coefficients and "material timescales"

The material autocorrelation coefficient can be calculated similarly to the material correlation defined by Saffman[3] as

$$R_{V_iV_j}(t, t_o) = \frac{\overline{V_i'(t - t_o)V_j'(t_o)}}{(\overline{V_i'^2(t - t_o)})^{1/2}(\overline{V_j'^2(t_o)})^{1/2}} \qquad i, j = x, y, z \tag{6}$$

The marker velocity at the time of marker release is used for the calculations of the autocorrelation coefficient presented in Figure 13. The overbar denotes ensemble average over the total

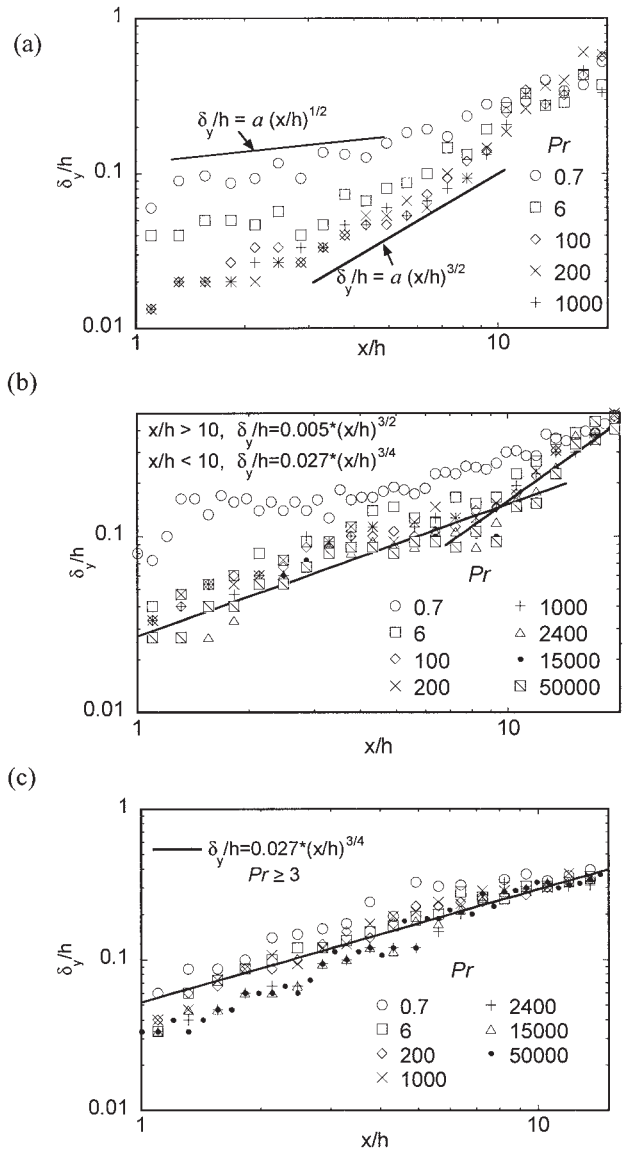

Figure 11. Plume half-width for Poiseuille channel flow.

(a) $y_o = 5$; (b) $y_o = 15$; (c) $y_o = 28.5$.

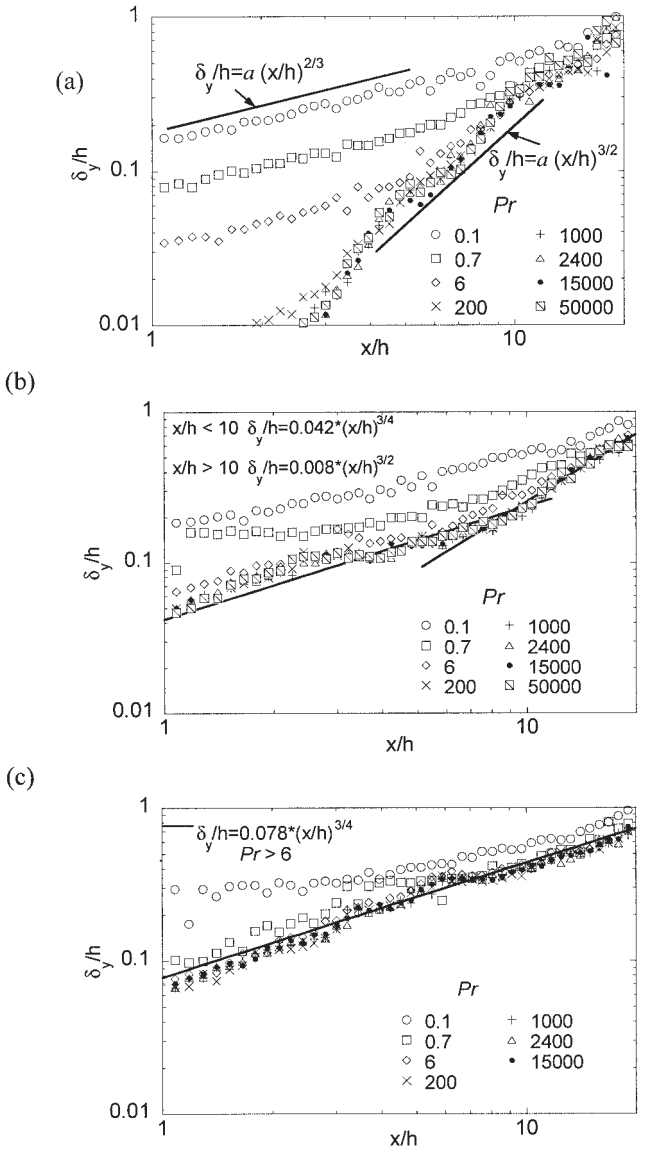

Figure 12. Plume half-width for Couette flow.

(a) $y_o = 5$; (b) $y_o = 15$; (c) $y_o = 28.5$.

number of markers in the flow field and the prime denotes Lagrangian velocity fluctuations, $V_i = V_i(t) - \overline{V}_i(t)$. Note here that $V_i(t)$ is the velocity of a fluid particle that is located at the same point as the scalar marker, as mentioned above in the LST section.

The streamwise-streamwise, $R_{V_xV_x}(t, t_o)$; the normal–normal, $R_{V_yV_y}(t, t_o)$; and the spanwise–spanwise, $R_{V_zV_z}(t, t_o)$, correlations are shown in Figures 13a, 13b, and 13c, respectively, for the case of channel flow and a source within the logarithmic region ($y_o = 75$). Figure 13 shows that the material autocorrelation coefficient does not depend on Pr for Pr $\geq$ 3 for sources in the logarithmic region of the channel flow. A measure of the difference between the material autocorrelation coefficient and the usual Lagrangian coefficient that can be calculated along the trajectories of fluid particles can be obtained by comparing the values in Figure 13 with the values of $R_{V_iV_i}$ for the highest Pr shown (Pr = 50,000) because fluid particles behave like markers with Pr $\rightarrow \infty$. For markers with small Pr, the coefficients are smaller, meaning that molecular diffusion quickly moves these markers off large fluid flow structures. In this respect, the effectiveness of turbulence mixing is diminished because the markers do not follow the turbulent flow eddies. It is important to note here that, although the effectiveness of turbulence to mix is diminished, the overall effective dispersion is enhanced when the Pr is small. The concept proposed by Saffman,[3] that the overall effective dispersion will be diminished as a result of molecular effects, is applicable to very small times, that is, $t \rightarrow 0$. Also, Figure 13 shows that total dispersion in the normal direction is more rapid, given that $R_{V_xV_x} > R_{V_zV_z} > R_{V_yV_y}$. Similar results are found for the Couette flow correlation coefficients, shown in Figure 14. However, the correlation coefficients are smaller for the Couette flow case, indicating more efficient total dispersion.

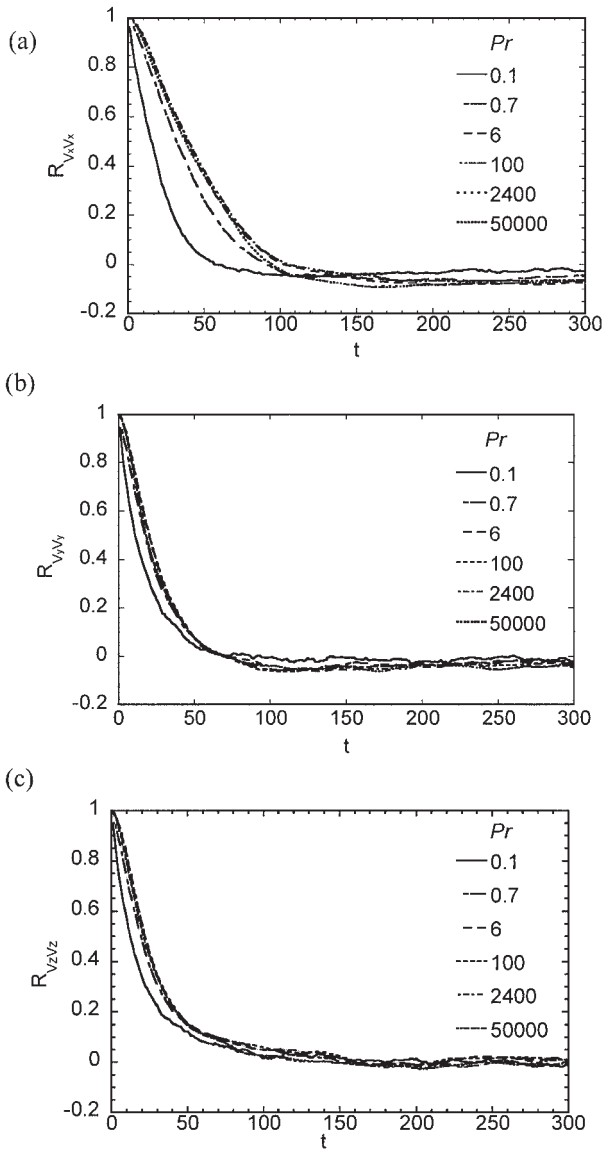

Figure 13. Material correlation coefficients as a function of Pr for markers released in Poiseuille flow.

(a) $R_{V_xV_x}$, $y_o = 75$; (b) $R_{V_yV_y}$, $y_o = 75$; (c) $R_{V_zV_z}$, $y_o = 75$.

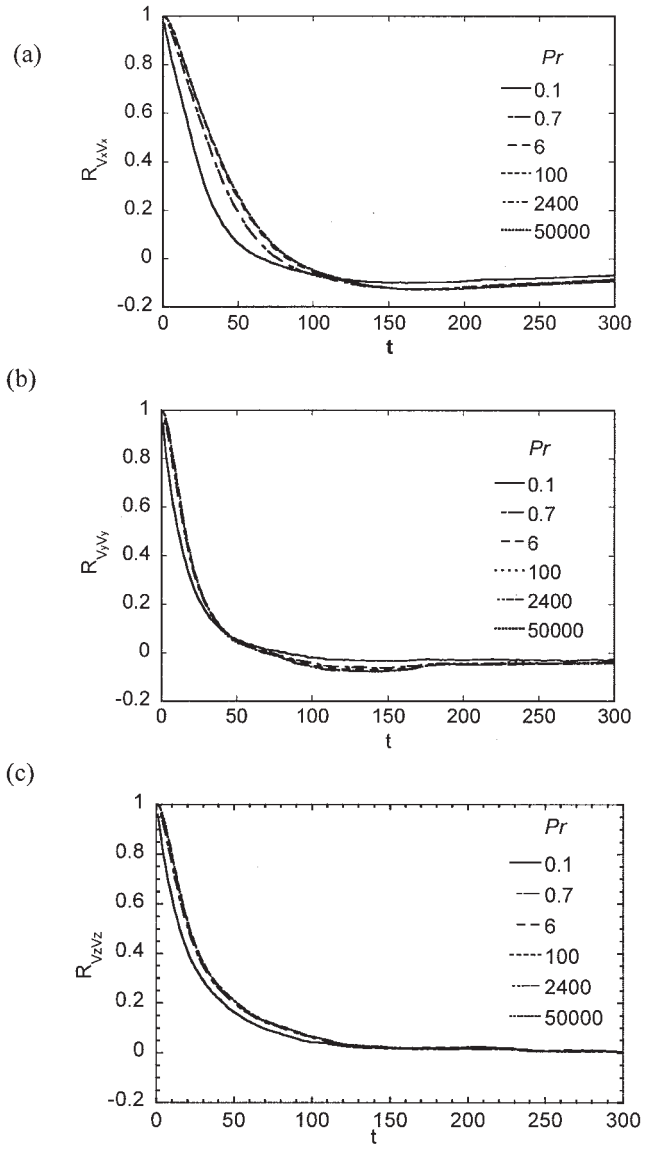

Figure 14. Material correlation coefficients as a function of Pr for markers released in Couette flow.

(a) $R_{V_xV_x}$, $y_o = 75$; (b) $R_{V_yV_y}$, $y_o = 75$; (c) $R_{V_zV_z}$, $y_o = 75$.

Figures 15a and 15b present the Lagrangian timescale as a function of source elevation for dispersion in the *y*-direction that can be calculated as

$$\tau_{Ly} = \int_{t_o}^{\infty} R_{V_yV_y}(t, t_o)dt \tag{7}$$

for Poiseuille and Couette flow, respectively. This timescale may be called the *material timescale* to differentiate it from the term *Lagrangian timescale*, which is usually reserved for the timescale of fluid particles moving without molecular diffusion. The material timescale in this case (that is, inhomogeneous, anisotropic turbulence) is expected to depend on the source elevation and, to some degree, on the Pr. The material correlation coefficient can be written as the material autocorrelation coefficient for the case of homogeneous turbulence, $(R_{V_yV_y})_H$, modified by a factor representing the effects of inhomogeneity. This factor may be assumed to have two components, one that depends on the location of the source, $(R_{V_yV_y})_{y_o}$, and a second one that includes the effects of the Pr, $(R_{V_yV_y})_{\mathrm{Pr}}$. The material correlation coefficient may then be written as

$$R_{V_yV_y} = (R_{V_yV_y})_H (R_{V_yV_y})_{y_o} (R_{V_yV_y})_{\mathrm{Pr}} \tag{8}$$

The factor $(R_{V_yV_y})_H$ is usually assumed to follow an exponential function[12,43]

$$(R_{V_yV_y})_H = e^{-t/\tau} \tag{9}$$

which gives $\tau = \tau_{Ly}$ when combined with Eq. 7 for the case of homogeneous turbulence. Considering that the term $[\overline{V_j^2(t_o)}]^{1/2}$ in the denominator of Eq. 6 is equal to the root mean square of the velocity fluctuations in the direction normal to the walls of the channel, *v*, and keeping a first-order dependency on the source location of the modification factor that accounts for the elevation of the source, one may write

$$(R_{V_yV_y})_{y_o} = A_1 + A_2\left(\frac{y_o}{h}\right)\left(\frac{1}{\nu}\right)_{y_o} \tag{10}$$

where A_1 and A_2 are constants. The physical meaning of A_1 is that $(R_{V_yV_y})_{y_o=0} = A_1$, so that Eq. 8 does not yield a zero value at $y_o = 0$. Note also that *v* depends on the distance from the

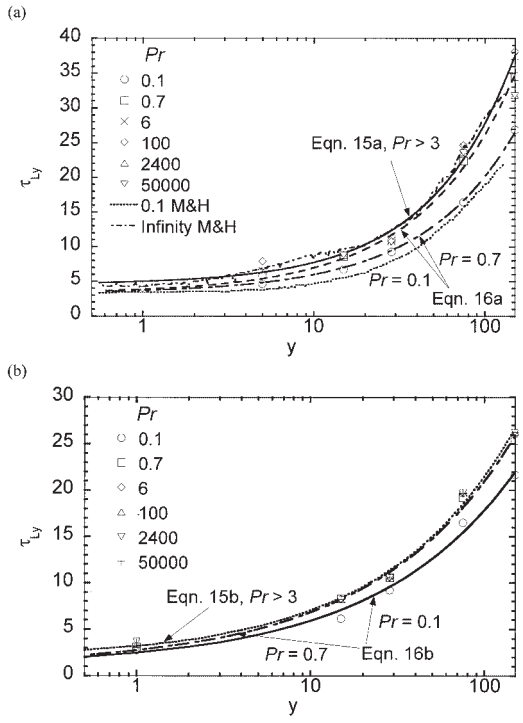

Figure 15. Material timescale as a function of the elevation of the point of release.

(a) Poiseuille flow (MH = data from Mito and Hanratty[10]); (b) Couette flow.

wall, in the form $v \sim (y/h)^s$ for small y (that is, $y < 30$, whereas for $y \to 0$ incompressibility implies $s = 2$), and v is almost constant for large y (that is, $y > 50$; see Figure 1b). Equation 10 can then be written as

$$(R_{V_yV_y})_{y_o} = A_1 + A_2\left(\frac{y_o}{h}\right)^{1-s} \tag{11}$$

where s is zero at large y_o. The Pr-dependent factor can be assumed to follow an exponential

$$(R_{V_yV_y})_{\mathrm{Pr}} = b_1\mathrm{Pr}^{b_2} \tag{12}$$

The exponential form can be justified because a Lagrangian correlation coefficient is related to the eddy diffusivity, and the eddy diffusivity in wall turbulence has an exponential dependency on the Pr (see Churchill[41]), especially for small Pr. Substituting Eqs. 9, 11, and 12 into Eq. 8 yields

$$R_{V_yV_y} = b_1\mathrm{Pr}^{b_2}e^{-t/\tau}[A_1 + A_2(y_o/h)^{1-s}] \tag{13}$$

Mito and Hanratty[10] studied the behavior of markers released at different elevations in a Poiseuille flow channel to calculate the associated material timescales (Pr = 0.1, 0.3, 1, and ∞). Their goal was to use these timescales to solve a modified Langevin equation for the prediction of the velocity field along the trajectories of the markers, and subsequently use that velocity field to predict the marker trajectories (in other words, they substituted the DNS velocity in an LST procedure with the velocity field resulting from the solution of the Langevin equation). The results in Figure 15a are in agreement with the findings of Mito and Hanratty[10] that there is a Pr effect for small Pr and that this effect is more pronounced close to the wall. The Couette flow results exhibit similar qualitative behavior. However, the values of the material timescale are smaller than those for Poiseuille flow. Substitution of Eq. 13 into Eq. 7 shows that the values of τ_{Ly} can be modeled with an equation of the form

$$\tau_{Ly} = B_1\mathrm{Pr}^{b_2}[A_1 + A_2(y_o/h)^{1-s}] \tag{14}$$

where B_1, b_2, A_1, A_2, and s are parameters that can be determined using regression. For medium and high Pr (Pr > 3) there is no Pr dependency ($b_2 = 0$), and the following relations are obtained:

Poiseuille Flow

$$\tau_{Ly} = 4.59 + 33.04(y_o/h)^{0.87} \qquad R^2 = 0.988 \tag{15a}$$

Couette Flow

$$\tau_{Ly} = 1.83 + 24.85(y_o/h)^{0.58} \qquad R^2 = 0.993 \tag{15b}$$

For small Pr, the material timescale exhibits a dependency on Pr, and the following relations are obtained:

Poiseuille Flow

$$\tau_{Ly} = (0.98\ \mathrm{Pr}^{0.13})[4.59 + 33.04(y_o/h)^{0.87}] \qquad R^2 = 0.997 \tag{16a}$$

Couette Flow

$$\tau_{Ly} = \mathrm{Pr}^{0.083}[1.83 + 24.85(y_o/h)^{0.58}] \qquad R^2 = 0.992 \tag{16b}$$

The regression results are shown in Figure 15. Note that the Pr dependency is stronger for Poiseuille flow ($b_2 = 0.13$ in Eq. 16a) than for Couette flow ($b_2 = 0.083$ in Eq. 16b). Comparing Eq. 14 with the above, the value of the exponent s is 0.13 for Poiseuille flow and 0.42 for Couette flow (a power approximation to the v profile yields values of s equal to 0.11 and 0.36 for channel flow and Couette flow, respectively, based on the data shown in Figure 1b).

The differences observed in Figure 15 between the two types of flow can be investigated further by examining the spectrum of the Lagrangian velocity covariance $C(t)$,

$$C_{ij}(t) = R_{V_iV_j}(t, t_o)(\overline{V_i'^2(t - t_o)})^{1/2}(\overline{V_j'^2(t_o)})^{1/2} \qquad i, j = x, y, z \tag{17}$$

which can be defined as

$$E(w) = \frac{1}{\pi}\int_{-\infty}^{+\infty} C(t)e^{-iwt}dt \tag{18}$$

The spectra $E(w)$ of the C_{yy} material covariance for markers released inside the viscous wall region are shown in Figures 16a and 16b for the cases of channel and Couette flows, respectively. Figures 17a and 17b present the spectra for the case of markers released in the outer region of the channel. As mentioned earlier regarding Eq. 9, the Lagrangian autocorrelation coefficient is usually assumed to follow an exponential function[12] of the form $R_i = \exp(-t/\tau_i)$ that is appropriate for homogeneous, isotropic turbulence and gives $R_i = 0.368$ when $t = \tau_i$. The spectrum that results using this function in Eq. 17 is also shown in Figures 16 and 17 (designated as "analytical") to show the effects of the turbulence structure on heat transfer. For release close to the wall (Figure 16), the differences in the spectra for different Pr are significant for small and medium Pr. The spectra become Pr independent for high Pr (>100). There are also differences between the actual spectrum and the exponential function arising from the presence of the wall and the anisotropies introduced by the wall.

For release in the logarithmic region (Figure 17), the spectrum shows differences at small wavenumbers for different Pr, indicating differences in the contribution to heat transfer arising from large turbulence scales. It is seen that the reason for which the mechanism of heat transfer depends on the Pr, when it does so, is that the turbulence velocity structures that contribute to heat transfer are different in each case. Integrating the spectrum $E(w)$ up to the first 10 frequencies ($w \leq 0.078125$), and dividing this integral to the value of the same integral for

Pr = 50,000, shows a ratio of 0.84 and 0.78 for channel flow and Pr = 100 and 0.7, respectively, when the point of release is at $y_o = 75$. For release in the center of the channel ($y_o = 150$), the value of the ratio is 0.88 and 0.84 for Pr values of 100 and 0.7, respectively. However, such differences are much smaller for Couette flow. In Couette flow, for release at $y_o = 75$, the ratio is 1.0 and 0.96 for Pr values of 100 and 0.7, respectively. For release at $y_o = 150$, the value of the ratio is 1.0 and 0.97 for Pr values of 100 and 0.7, respectively. It appears that within the constant-stress region (which covers almost the whole channel in the Couette flow case) all the velocity scales contribute almost equally to the dispersion of heat, apart from the case of low Pr, that is, Pr = 0.1. Furthermore, the values of the spectral function are higher for the Couette flow case, showing that similar frequency structures can be more dispersive in Couette flow than in channel flow. The fundamental reason for the observed differences in dispersion between different types of flow appears to be the intensity of the large-scale velocity events (that is, the magnitude of the fluctuations), but not their duration.

Conclusions

The behavior of instantaneous and continuous line sources of heat or mass at different locations of turbulent plane Poiseuille and plane Couette flow has been investigated in this work using Lagrangian scalar tracking. The effect of the turbulence structure and of different Pr in turbulent transport has also been studied. The range of the fluid molecular Prandtl number extended from 0.1 to 50,000. The numerical results agreed well with previous experimental measurements for the case of a plume, as well as with previous Lagrangian simulations for the case of the Lagrangian timescale for channel flow.

With respect to the turbulent dispersion dependency on Pr, it was found that it is important when the molecular Pr is comparable to the turbulent Pr, in agreement with previous work and theoretical expectations. The material autocorrelation function and the associated material timescale were Pr independent for Pr $\geq$ 3. However, when the source location was close to the wall and, more specifically, within the viscous wall sublayer, the effects of Pr were significant. The assumption that the Lagrangian velocity of scalar markers is independent of Pr within the constant stress region was found to be invalid. Descriptive correlations for the material timescale have been calculated (Eqs. 15 and 16) for low and high Pr. It was also found that dispersion is stronger in the plane Couette flow case relative to the plane channel flow, indicating enhancement of turbulent dispersion in the constant stress region and thus in the logarithmic region. The difference is attributed to the large-scale velocity events that contribute to heat transfer. In general, turbulent dispersion is different in different turbulent velocity fields because the large scale structures of these turbulent velocity fields are different.

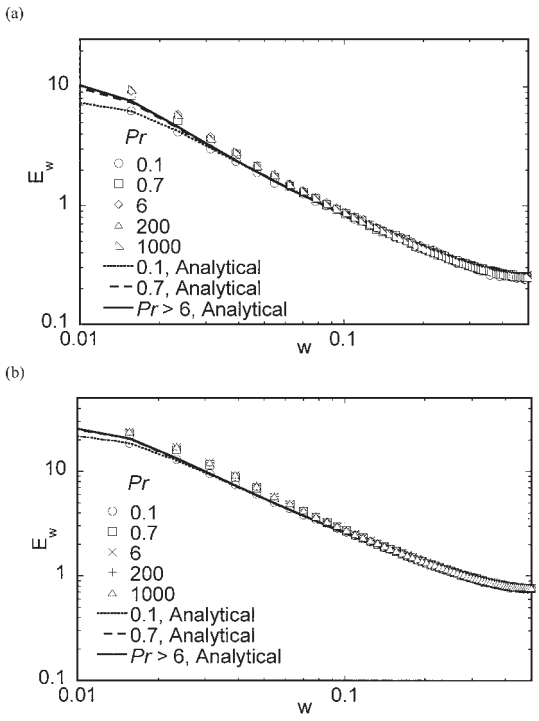

Figure 17. Spectrum of the material autocorrelation coefficient $R_{V_yV_y}$ for high Pr and markers released inside the logarithmic region ($y_o = 75$).

(a) Poiseuille flow; (b) Couette flow. The lines marked "Analytical" show the spectrum of $R_{V_yV_y} = \exp(-t/\tau_{Ly})$.

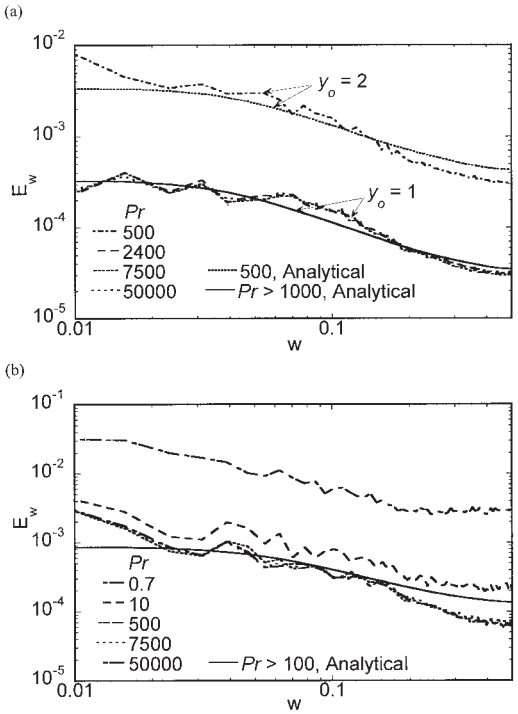

Figure 16. Spectrum of the material autocorrelation coefficient $R_{V_yV_y}$ for high Pr and markers released inside the viscous wall region ($y_o = 1$).

(a) Poiseuille flow; (b) Couette flow. The lines marked "Analytical" show the spectrum of $R_{V_yV_y} = \exp(-t/\tau_{Ly})$.

Acknowledgments

The support of NSF under CTS-0209758 is gratefully acknowledged. This work was also supported by the National Computational Science Alliance under CTS990021N, used the NCSA IBMp690 and the NCSA SGI/CRAY Origin2000. Computational support was also offered by the

University of Oklahoma Center for Supercomputing Education and Research (OSCER).

Literature Cited

1. Taylor GI. Diffusion with continuous movements. *Proc Lond Math Soc*. 1921;24A:196-212.
2. Einstein A. Uber die von der molekular-kinetischen Theorie der Warme geforderte Bewegung von in ruhenden Flussigkeiten suspendierten Teilchen. *Ann Phys*. 1905;17:549.
3. Saffman PG. On the effect of the molecular diffusivity in turbulent diffusion. *J Fluid Mech*. 1960;8:273-283.
4. Batchelor GK. Diffusion from sources in a turbulent boundary layer. *Arch Mech Stos*. 1964;3:661-670.
5. Shlien DJ, Corrsin S. Dispersion measurements in a turbulent boundary layer. *Int J Heat Mass Transfer*. 1976;19:285-295.
6. Fackrell JE, Robins AG. Concentration fluctuations and fluxes in plumes from point sources in a turbulent boundary layer. *J Fluid Mech*. 1982;117:1-26.
7. Kontomaris K, Hanratty TJ. Effect of molecular diffusivity on point source diffusion in the center of a numerically simulated turbulent channel flow. *Int J Heat Mass Transfer*. 1994;37:1817-1828.
8. Papavassiliou DV, Hanratty TJ. Transport of a passive scalar in a turbulent channel flow. *Int J Heat Mass Transfer*. 1997;40:1303-1311.
9. Mitrovic BM, Papavassiliou DV. Transport properties for turbulent dispersion from wall sources. *AIChE J*. 2003;49:1095-1108.
10. Mito Y, Hanratty TJ. Lagrangian stochastic simulation of turbulent dispersion of heat markers in a channel flow. *Int J Heat Mass Transfer*. 2003;46:1063-1073.
11. Papavassiliou DV. Scalar dispersion from an instantaneous line source at the wall of a turbulent channel for medium and high Prandtl number fluids. *Int J Heat Fluid Flow*. 2002;23:161-172.
12. Hanratty TJ. Heat transfer through a homogeneous isotropic turbulent field. *AIChE J*. 1956;2:42-45.
13. Kontomaris K, Hanratty TJ, McLaughlin JB. An algorithm for tracking fluid particles in a spectral simulation of turbulent channel flow. *J Comput Phys*. 1993;103:231-242.
14. Papavassiliou DV, Hanratty TJ. The use of Lagrangian methods to describe turbulent transport of heat from the wall. *Ind Eng Chem Res*. 1995;34:3359-3367.
15. Ponoth SS, McLaughlin JB. Numerical simulation of mass transfer for bubbles in water. *Chem Eng Sci*. 2000;55:1237-1255.
16. Papavassiliou DV. Turbulent transport from continuous sources at the wall of a channel. *Int J Heat Mass Transfer*. 2002;45:3571-3583.
17. Hasegawa Y, Kasagi N. The effect of Schmidt number on air–water interface mass transfer. Proc of the 4th Int Conf on Multiphase Flow 2001, New Orleans, LA (CD-ROM), May; 2001.
18. Hasegawa Y, Kasagi N, Hanazaki H. Direct numerical simulation of passive scalar transfer across a turbulent gas–liquid interface. Proc of the 1st Int Symp on Advanced Fluid Information, Sendai, Japan, October; 2001:696-701.
19. Kim J, Moin P. Transport of passive scalars in a turbulent channel flow. In: Andre J-C, Cousteix J, Durst F, Launder, Schmidt FW, Whitelaw JH, eds. *Turbulent Shear Flows*. Vol. 6. Berlin, Germany: Springer-Verlag;1989:85-96.
20. Lyons SL, Hanratty TJ, McLaughlin JB. Direct numerical simulation of passive heat transfer in a turbulent channel flow. *Int J Heat Mass Transfer*. 1991;34:1149-1161.
21. Kasagi N, Shikazono N. Contribution of direct numerical simulation to understanding and modeling turbulent transport. *Proc R Soc Lond A Phys Sci*. 1995;451:257-292.
22. Kawamura H, Abe H, Matsuo Y. DNS of turbulent heat transfer in channel flow with respect to Reynolds and Prandtl number effects. *Int J Heat Fluid Flow*. 1999;20:196-207.
23. Na Y, Papavassiliou DV, Hanratty TJ. Use of direct numerical simulation to study the effect of Prandtl number on temperature fields. *Int J Heat Fluid Flow*. 1999;20:187-195.
24. Tiselj I, Pogrebnyak E, Changfeng L, Mosyak A, Hetsroni G. Effect of wall boundary condition on scalar transfer in a fully developed turbulent flume. *Phys Fluids*. 2001;13:1028-1039.
25. Liu C-H. Turbulent plane Couette flow and scalar transport at low Reynolds number. *J Heat Trans-T ASME*. 2003;125:988-998.
26. Debusschere B, Rutland CJ. Turbulent scalar transport mechanisms in plane channel and Couette flows. *Int J Heat Mass Transfer*. 2004;47:1771-1781.
27. Antonia RA, Orlandi P. Effect of Schmidt number on small-scale passive scalar turbulence. *Appl Mech Rev*. 2003;56:615-632.
28. Yeung PK, Xu S, Sreenivasan KR. Schmidt number effects on turbulent transport with uniform mean scalar gradient. *Phys Fluids*. 2002;14:4178-4191.
29. Nieuwstadt FTM, Brethouwer G. Turbulent transport and mixing. In: Dopazo C et al., eds. *Advances in Turbulence VIII*. Barcelona, Spain: CIMNE; 2000:133-140.
30. Brethouwer G, Hunet JCR, Nieuwstadt FTM. Micro-structure and Lagrangian statistics of the scalar field with a mean gradient in isotropic turbulence. *J Fluid Mech*. 2003;474:193-225.
31. Lyons SL, Hanratty TJ, McLaughlin JB. Large-scale computer simulation of fully developed turbulent channel flow with heat transfer. *Numer Methods Fluids*. 1991;13:999-1028.
32. Guenther A, Papavassiliou DV, Warholic MD, Hanratty TJ. Turbulent flow in a channel at low Reynolds number. *Exp Fluids*. 1998;25:503-511.
33. Papavassiliou DV, Hanratty TJ. Interpretation of large scale structures in a turbulent plane Couette flow. *Int J Heat Fluid Flow*. 1997;18:55-69.
34. Komminaho J, Lundbladh A, Johansson AV. Very large structures in plane turbulent Couette flow. *J Fluid Mech*. 1996;320:259-285.
35. Mitrovic BM, Papavassiliou DV. Effects of a first-order chemical reaction on turbulent mass transfer. *Int J Heat Mass Transfer*. 2004;47:43-61.
36. Na Y, Hanratty TJ, Liu JC. The use of DNS to define stress producing events for turbulent flow over a smooth wall. *Flow Turbul Combust*. 2001;66:495-512.
37. Kasagi N, Tomita Y, Kuroda A. Direct numerical simulation of passive scalar field in a turbulent channel flow. *J Heat Trans-T ASME*. 1992;114:598-606.
38. Kawamura H, Oshaka K, Abe H, Yamamoto K. DNS of turbulent heat transfer in channel flow with low to medium-high Prandtl number fluid. *Int J Heat Fluid Flow*. 1998;19:482-491.
39. Dong YH, Lu XY, Zhuang. An investigation of the Prandtl number effect on turbulent heat transfer in channel flows by large eddy simulation. *Acta Mech*. 2002;159:39-51.
40. Weigand B, Ferguson JR, Crawford ME. An extended Kays and Crawford turbulent Prandtl number model. *Int J Heat Mass Transfer*. 1997;40:4191-4196.
41. Churchill SW. Progress in the thermal sciences: AIChE Institute Lecture. *AIChE J*. 2000;46:1704-1722.
42. Page F Jr, Schlinger WG, Breaux DK, Sage BH. Point values of eddy conductivity and viscosity in uniform flow between parallel plates. *Ind Eng Chem*. 1952;44:424-430.
43. Pasquill F. *Atmospheric Diffusion*. 2nd Edition. Chichester, UK: Halsted Press; 1974.
44. Lee MJ, Kim J. The structure of turbulence in a simulated plane Couette flow. Proc of the 8th Symp on Turbulent Shear Flows. Paper 5-3. Munich, Germany; 1991.
45. Aydin M, Leutheusser HJ. Plane-Couette flow between smooth and rough walls. *Exp Fluids*. 1991;11:302-312.
46. Robertson JM, Johnson HF. Turbulence structure in plane Couette flow. *Proc ASCE J Eng Mech Div*. 1970;96:1171-1182.

Manuscript received Feb. 11, 2004, and revision received Jan. 12, 2005.